Effect of temperature and configurational disorder on the electronic band gap of boron carbide from first principles

A. Ektarawong,[1,*] S. I. Simak,[1] and B. Alling[1,2]

[1]*Theoretical Physics Division, Department of Physics, Chemistry and Biology (IFM), Linköping University, SE-581 83 Linköping, Sweden*

[2]*Max-Planck-Institut für Eisenforschung GmbH, Max-Planck Strasse 1, 40237 Düsseldorf, Germany*

(Received 23 May 2018; revised manuscript received 2 September 2018; published 19 October 2018)

The overestimation, rather than the usual underestimation, of the electronic band gap at 0 K of boron carbide with the ideally stoichiometric composition of B_4C, represented by $B_{11}C^p$(CBC), in density functional theory calculations is one of the outstanding controversial issues in the field of icosahedral boron-rich solids. Using a first-principles approach, we explore the effect of temperature and configurational disorder on the electronic band gap of B_4C. *Ab initio* molecular dynamics simulations are performed to account for the effects of vibrational disorder. The results reveal that the volumetric thermal expansion as well as the thermally induced configurational disorder of icosahedral C^p atoms residing in the $B_{11}C^p$ icosahedra have a minimal impact on the band gap of B_4C, while a major decrease of the band gap is caused by explicit atomic displacements, induced by lattice vibrations. At 298 K, the band gap of B_4C is overestimated, as compared to the experimental value, by approximately 31%. However, configurational disorder induced by introducing a small fraction of B_{12}(CBC) and $B_{12}(B_4)$ into a matrix of $B_{11}C^p$(CBC) to make the composition of boron carbide approximately $B_{4.3}C$, claimed to be the carbon-rich limit of the material in experiment, leads to a smaller band gap due to the appearance of midgap states. These results can explain at least a part of the previous discrepancies between theory and experiments for the band gap of boron carbide.

DOI: 10.1103/PhysRevMaterials.2.104603

I. INTRODUCTION

Boron carbide is a binary solid solution of carbon in boron, whose homogeneity range extends from approximately 8 to 20 at. % C [1–3]. Revealed by x-ray and neutron diffraction studies [4–7], the crystal structure of boron carbide is composed of 12-atom icosahedra and intericosahedral chains. The icosahedra are situated at the vertices of a rhombohedral unit cell ($R\bar{3}m$), and the adjacent icosahedra are bridged by the intericosahedral chains. Despite being a candidate for high-temperature electronic and thermoelectric applications [8–11], several properties, relevant to such utilization, particularly atomic configuration and electronic properties, are still undecided and debated within the scientific community. This has been highlighted by large inconsistencies between experiment and theoretical predictions. One of the discrepancies is the prediction of a metallic state for $B_{13}C_2$, represented by B_{12}(CBC), due to its electron deficiency [12–14]. This is in contrast with the fact that boron carbide is a semiconductor over the whole solubility range [15,16]. Another discrepancy is the overestimation of the electronic band gap of B_4C, given by $B_{11}C^p$(CBC), where p denotes the polar site of the icosahedron [17–19], by standard density functional theory (DFT) calculations, which is known to practically always underestimate the band gaps of other materials by 30–50 % owing to the approximation of the electronic exchange-correlation functionals [20–22]. The electronic band gap of carbon-rich boron carbide with the composition of around $B_{4.3}C$, obtained from optical measurements, has been reported to be 2.09 eV at ambient conditions [23], while the standard DFT-derived band gap of boron carbide, based on the structural model of the ideally stoichiometric B_4C or $B_{11}C^p$(CBC), ranges from 2.6 up to 3.0 eV [17–19,24]. It is worth mentioning here that the use of the hybrid functional to account for the exchange-correlation effects [25–27], generally providing a better description of electronic band gaps for semiconductors as compared to the standard DFT calculations, results in a band gap as large as 4.13 eV for $B_{11}C^p$(CBC) [19]. Such a large inconsistency between the theoretically predicted band gap of B_4C and the experimental one may be attributed to the absence of localized midgap states induced by boron/carbon substitutional disorder [2,28,29], which has so far not been explicitly taken into account in the theoretical simulations.

Recent theoretical studies demonstrated that electron deficiency in the idealized B_{12}(CBC) can be compensated either by a thermally activated configurational disorder of boron and carbon atoms [30] or via a combination of different intericosahedral chain motifs, for example, the linear CBC and CBCB as well as rhombic B_4 chains [31–35]. The latter has been suggested from the thermodynamics aspect to be the most plausible explanation of how boron carbide retains its semiconducting state within the homogeneity range. The overestimation of the band gap of B_4C might also be because of the configurational disorder of B and C atoms, induced by high concentrations of low-energy defects, and/or the combination of different icosahedral and chain motifs, which is analogous to the case of B_{12}(CBC). The ideas have been inspired by the experimental studies [36,37], seemingly suggesting that $B_{4.3}C$ is the carbon-rich limit of the homogeneity range, and thus

*annop.ektarawong@liu.se

the ideally stoichiometric composition of B_4C may not exist in nature. Another possibility, which could be the cause of overestimating the band gap of B_4C, might be attributed to the atomic displacements, induced by the lattice vibrations, which were not explicitly taken into account in the previous band-gap calculations. The impact of such atomic displacements can be significantly strong for materials comprised of light elements, particularly boron carbide. To the best of our knowledge, the influence of temperature-induced atomic displacements on the band gap of boron carbide has not been explored.

With the aim of resolving the band-gap problem, we probe using a first-principles approach the effect of temperature and configurational disorder induced by low-energy B/C substitutional defects on the band gap of carbon-rich boron carbides, in particular B_4C. In this work, we perform *ab initio* molecular dynamics (AIMD) simulations, in combination with the DFT calculations, to derive the band gap as a function of temperature. The simulations show that the volumetric thermal expansion has a minimal impact on the band gap of the material, while a major decrease of the band gap is caused by the explicit atomic displacements induced by the lattice vibrations. In addition, we find that adding a small fraction of B_{12}(CBC) and $B_{12}(B_4)$ into a matrix of $B_{11}C^p$(CBC) to achieve the composition of approximately $B_{4.3}C$ leads to a smaller band gap because of the appearance of the midgap states. These findings are in line with the normal observation of a systematic underestimation of experimental band gaps in density functional theory calculations for most of other materials [20–22].

II. METHODOLOGY

A. Structural models of B_4C and $B_{4.3}C$

First, it is worth emphasizing here that experimentally identifying defects, inducing the configurational disorder of boron and carbon atoms, for boron carbide at any given composition and temperature has still been a formidable challenge. This can be attributed not only to the complexity of the icosahedral structure but also to the similar characteristics of boron and carbon atoms, i.e., the atomic form factor for x-ray diffraction [38] and the nuclear scattering cross sections (^{11}B and ^{12}C) for neutron diffraction [7,39]. As a consequence, there has so far been no unambiguous experimental spectroscopic evidence to explicitly characterize structural defects existing in boron carbide, and several investigations of defects inducing configurational disorder in boron carbide have by far been based mostly on the theoretical simulations [2,19,30–35,40–44]. The structural model of the ideally stoichiometric B_4C is given by $B_{11}C^p$ icosahedra and linear CBC chains, as it has been demonstrated by several theoretical studies [17,19,40–42] to be the most favorable configuration from the thermodynamics aspect. To examine the impact of temperature and configurational disorder of B and C atoms induced by high concentrations of low-energy B/C substitutional defects on the band gap of the material, we consider in the present work two atomic configurations of B_4C. Those are (1) *ordered* B_4C, where the C^p atoms are well oriented, occupying the same polar position for every icosahedron, and (2) *disordered* B_4C, where the C^p atoms configurationally disorder at the polar sites without the formation of inter- and intraicosahedral bonds between the C^p atoms. The former has been demonstrated by several independent first-principles calculations to exhibit the lowest-energy configuration at $T = 0$ K [17,19,40–42], and it thus has presumably been believed to be the ground state for B_4C, while the latter has been predicted to be favored with respect to the ordered one at elevated temperature [19,43,45]. As demonstrated in our previous work [45], the energy difference between the ordered and disordered B_4C at $T = 0$ K, taking into account the influence of the zero-point motion, is 72 meV per unit cell, accordingly resulting in the mean-field-estimated order-disorder transition temperature of 730 K. It is worth noting that the same configurational transition from the ordered to the disordered states of B_4C has been independently predicted by Yao *et al.* [43] to take place at $T \geqslant 717$ K, in line with our prediction [45]. In the present work, we use simulation boxes containing 120 atoms, arranged in a supercell of $2 \times 2 \times 2$ primitive rhombohedral unit cells, for both ordered and disordered B_4C.

The structural model of the off-stoichiometric $B_{4.3}C$ is, on the other hand, obtained by introducing a small fraction of structural defects, i.e., B_{12}(CBC) and $B_{12}(B_4)$, into a matrix of $B_{11}C^p$(CBC). Among numerous types of structural defects, B_{12}(CBC) and $B_{12}(B_4)$ have been chosen for the following reasons. First, first-principles studies of boron carbide [12,40,41] demonstrated that, as the carbon content goes lower than 20 at. %, the C^p atoms residing in the $B_{11}C^p$ icosahedra rather than C atoms residing in the linear CBC chains tend to be replaced by B atoms, hence resulting in the formation of electron-deficient B_{12}(CBC). Second, recent theoretical works on boron carbide [31–35] revealed that entirely compensating for the electron deficiency in B_{12}(CBC) through the addition of $B_{12}(B_4)$, in which the B_{12}(CBC)-to-$B_{12}(B_4)$ ratio is 2, can considerably lower the total energy of the material. We note that the rhombic B_4 chains were originally proposed by Yakel [5], based on the x-ray diffraction data of boron-rich boron carbide, and furthermore, most recently the existence of rhombic chains was observed experimentally by Rasim *et al.* [34] through high-resolution transmission electron microscopy of boron carbide, reasonably justifying the structural model of $B_{4.3}C$ employed in the present work. For this reason, we deduce that the atomic structure of $B_{4.3}C$ is composed of 90% $B_{11}C^p$(CBC), 6.67% B_{12}(CBC), and 3.33% $B_{12}(B_4)$, constructed within $5 \times 3 \times 2$ primitive rhombohedral unit cells (451 atoms). It is also worth noting that structural models of boron carbide based on a combination of $B_{11}C^p$(CBC), B_{12}(CBC),and $B_{12}(B_4)$ were previously considered by Shirai *et al.* [31], who discussed the boron-rich boron carbide $B_{6.5}C$. A detailed discussion about the energetics of the structural model of $B_{4.3}C$ considered in the present work with respect to B_4C is provided in Sec. III B.

B. Computational details

In the present work, the volume, cell shape, and internal atomic coordinates of B_4C and $B_{4.3}C$ are fully optimized through the DFT calculations, employing the projector augmented wave (PAW) method [46] as implemented

in the Vienna Ab initio Simulation Package (VASP) [47,48] and the generalized gradient approximation (GGA) proposed by Perdew, Burke, and Ernzerhof (PBE96) [49] for the exchange-correlation functional. The plane-wave energy cutoff of 400 eV is used, and the Monkhorst-Pack **k**-point mesh [50] is chosen for the Brillouin zone integration. For all DFT calculations, we also ensure that the calculated total energies of the considered structural models are converged with respect to both the energy cutoff and the density of the **k**-point grids.

To inspect the influence of thermal expansion on the band gap of B_4C, we derive the temperature-dependent volumetric thermal expansion coefficients (TECs) of both ordered and disordered B_4C using the quasiharmonic approximation, as implemented in the PHONOPY package [51,52].

To estimate the band gaps of B_4C and $B_{4.3}C$ at $T > 0$ K, we employ the AIMD simulations to take into account the explicit atomic displacements induced by the lattice vibrations. In the present work, the simulations are carried out using the canonical ensemble (NVT) to control the temperature of the simulations, where we choose the standard Nosé thermostat [53] as implemented in VASP with the default Nosé mass set by VASP, and the Brillouin zone sampling is limited to the Γ point. For this particular case, the band gaps of B_4C and $B_{4.3}C$ are estimated at $T \approx 500$, 1000, 1500, 2000, and 2250 K. First, the materials are heated to the temperature of interest within 1 ps and then equilibrated for 20 ps with a time step of 1 fs. The electronic density of states (DOS) is calculated with higher accuracy at every 0.5 ps during the equilibration procedure by using the tetrahedron method for the Brillouin zone integration [54] and the $7 \times 7 \times 7$ Monkhorst-Pack **k**-point mesh for sampling of the Brillouin zone.

Since the DOS and thus the band gap (E_g) are different at each time step, influenced by the atomic displacements and the fluctuations of the temperature around the desired one during the AIMD simulations, we determine at each temperature of interest the cumulative unweighted averages of the band gap and the temperature over the 40 snapshots, obtained at every 0.5 ps of the equilibration. Figure 1 illustrates the instantaneous value of E_g of ordered B_4C, calculated at every 0.5 ps of the AIMD simulations at 500 K and the corresponding cumulative average, ensuring that the result is properly converged with respect to the number of snapshots.

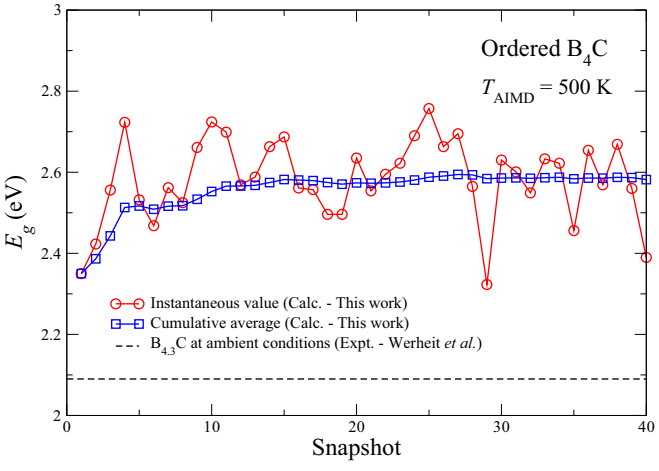

FIG. 1. Instantaneous value (open red circles) and cumulative average (open blue squares) of the band gap (E_g) of ordered B_4C at each snapshot, obtained from the *ab initio* molecular dynamics (AIMD) simulations at 500 K. The experimental band gap, derived from the optical measurements of $B_{4.3}C$ at ambient conditions [23] (dashed black line), is given for comparison.

III. RESULTS AND DISCUSSION

A. Influences of temperature and configurational disorder on electronic band gap of B_4C

Figure 2 displays the volumetric TEC of ordered and disordered B_4C as a function of temperature, derived from the quasiharmonic approach. We find the TECs of the two phases of B_4C behave similarly to one another. At $T < 700$ K, the TECs of the two phases are practically identical, while at $T > 2000$ K, the difference between them is smaller than 3%. Our calculated TECs are also in good agreement with the experimental TEC extracted from the volume expansion measurements of carbon-rich boron carbide by using high-temperature x-ray diffraction [55]. For this particular case, we use the fifth-degree polynomial function to fit the measured data points of the volume expansion temperature, reported by Yakel [55] in the temperature range of 285 to 1213 K. Such consistency validates our estimation of TEC for B_4C using the quasiharmonic approximation. It should be noted that the anomalous TEC of carbon-rich boron carbide, measured also by high-temperature x-ray diffraction, was previously reported by Tsagareishvili *et al.* [56]. It was, however, of the same order of magnitude as compared to that of Yakel [55] and our calculations.

To ensure that our simulations of E_g of B_4C, derived from the AIMD simulations, are also converged with respect to the size of the simulation box, we plot a histogram (see Fig. 3) showing the distribution of E_g of ordered B_4C at about 2000 K, obtained from the AIMD simulations done within the simulation boxes of $2 \times 2 \times 2$ (120 atoms) and $3 \times 3 \times 3$ (405 atoms) primitive rhombohedral unit cells. We find that

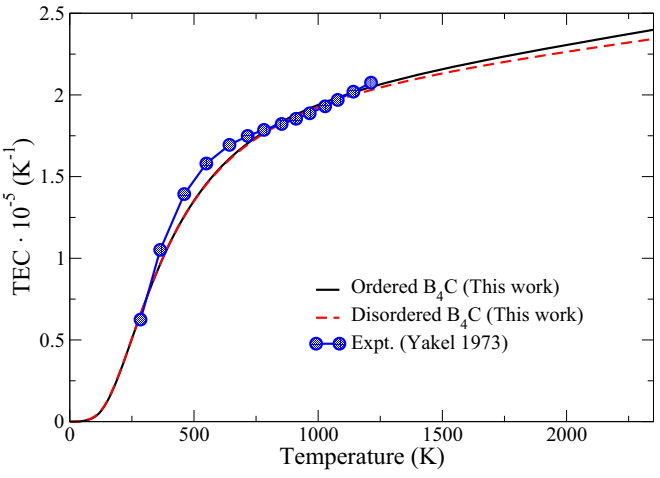

FIG. 2. Volumetric thermal expansion coefficient (TEC) of ordered and disordered B_4C as a function of temperature, calculated at the quasiharmonic level. Comparison is made with the experimental data, obtained from high-temperature x-ray diffraction methods [55].

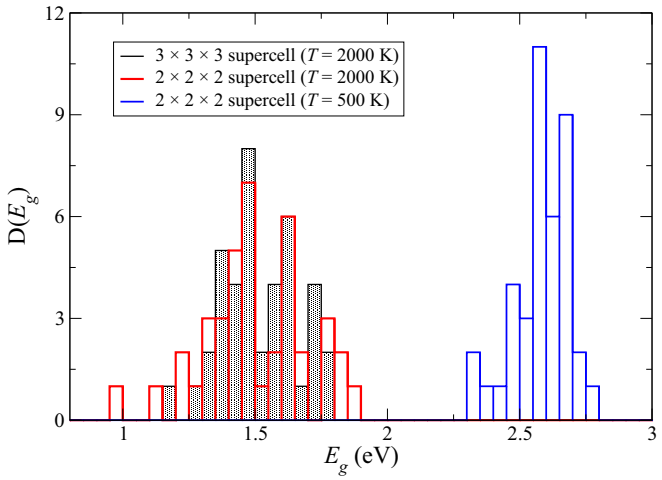

FIG. 3. Distribution of the band gap (E_g) of ordered B_4C, obtained from the AIMD simulations, equilibrated at 500 and 2000 K within the simulation boxes of $2 \times 2 \times 2$ (120 atoms) and $3 \times 3 \times 3$ (405 atoms).

the distributions of the band gap $D(E_g)$ obtained from the two different sizes of the AIMD simulation boxes are similar to one another, thus confirming the convergence of the band-gap calculations with respect to the simulation box size. We also provide in Fig. 3 the distribution of E_g of ordered B_4C at about 500 K, done within the simulation boxes of $2 \times 2 \times 2$ primitive rhombohedral unit cells (120 atoms) for comparison purposes. As can be seen from Fig. 3, the distribution of E_g of ordered B_4C equilibrated at about 2000 K is, apart from the systematic shift toward smaller band gaps, more statistically dispersed than that equilibrated at about 500 K. This is attributed to a higher degree of vibrational disorder as the temperature increases.

Our simulations reveal that the volumetric thermal expansion has a minimal impact on the band gap of B_4C, as can be seen from Fig. 4(a) illustrating the mean values of E_g of ordered B_4C, evaluated from AIMD simulations equilibrated at 500, 1000, 1500, 2000, and 2250 K, with and without considering the effect of thermal expansion. The same goes for disordered B_4C (not shown). The thermally induced configurational disorder of B and C atoms has, in a similar manner to the volumetric thermal expansion, also a minimal impact on the band gap of B_4C, as illustrated by the comparison of mean E_g versus T between ordered and disordered B_4C [Fig. 4(b)]. Instead, it seemingly shows that a major decrease of E_g is caused by lattice vibrations inducing the explicit displacements of atoms from their equilibrium positions during the simulations. As for B_4C, we observe that the mean value of E_g decreases linearly with respect to the temperature. We also observe that the electronic density of states of disordered B_4C, irrespective of temperature, behaves similarly to that of ordered B_4C. For illustrative purposes, Fig. 5 displays the density of states of ordered and disordered B_4C at 0 and 2000 K.

At 0 K, our estimated band gap of B_4C is 2.98 (2.95) eV for the ordered (disordered) phase, which is in line with the calculations previously reported in the literature [14,17,18], while at room temperature (298 K), the band gaps of B_4C (both ordered and disordered phases) are estimated in our case to be about 2.74 eV. We note that, in the present work, the effect of phonon-induced zero-point renormalization on the electronic band gaps of semiconductor materials has been neglected. As demonstrated in the previous works [57–59], the effect of zero-point renormalization on the band gaps of light-element semiconducting materials, such as diamond, hexagonal, and cubic boron nitrides, can cause a significant reduction of the band gap by up to 0.6 eV. In the case of boron carbide, the zero-point renormalization on the band gap could also be of similar magnitude and one can thus expect that, at room temperature, the calculated band gap of B_4C would reduce additionally as compared to the effect of classical vibrational disorder and might be found to be around 2.2 eV, still higher than the experimental value of 2.09 eV derived from the optical measurements of $B_{4.3}C$ [23]. It is also worth underlining that, in the present work, the band gaps of B_4C have been obtained from the standard DFT calculations in which the generalized gradient approximation [49] has been employed to estimate the electronic exchange-correlation effects. The use of such an approximation is known to severely underestimate the band gaps of semiconductors and insulators of the order of 30–50% or more [20–22]. Indeed, we found in our previous work [19] that when using the hybrid functional [25–27], known to give a more accurate description of band gaps, we obtained a value of 4.13 eV for ordered B_4C. Thus, taking into account the behavior of the generalized gradient approximation, even with the effect of phonon-induced zero-point renormalization, the calculated band gap of B_4C is still considerably too high. These findings imply that the theoretical band gaps of carbon-rich boron carbide, estimated from the structural model of the ideally stoichiometric B_4C, i.e., $B_{11}C^p$(CBC), cannot provide a quantitative agreement with the experiment, even though the temperature effect as well as the relevant configurational disorder of B and C atoms, induced by high concentrations of low-energy B/C substitutional defects, have been taken into consideration, as demonstrated in the present section.

In the case of B_4C, it is theoretically feasible to achieve a smaller band gap of ~2 eV, or less, due to the appearance of defect-induced gap states. As demonstrated by Dekura *et al.* [60], swapping the C^p atom residing in the $B_{11}C$ icosahedron with the middle-chain B atom of the CBC chain to form B_{12}(CCC) results in the formation of midgap states at about 1.6 eV above the valence-band edge. Furthermore, Ektarawong *et al.* [19] recently showed that for B_4C, even without the effect of phonon-induced zero-point renormalization, the gap states take place at about 2 eV above the valence-band edge if the configuration of the C^p atoms is highly disordered, leading to the formation of either intericosahedral or intraicosahedral C^p-C^p bonds. Though the configurations of B_4C, considered by Dekura *et al.* [60] and Ektarawong *et al.* [19], can result in a smaller band gap due to the appearance of the gap states and yield a better agreement compared to the experiment, they are very high in energy with respect to ordered B_4C and are thus disregarded by thermodynamics considerations [19,41].

Rather than semiconducting properties as observed in crystalline B_4C, amorphous B_4C has been predicted, using the melt-quenching approach based on AIMD simulations, to

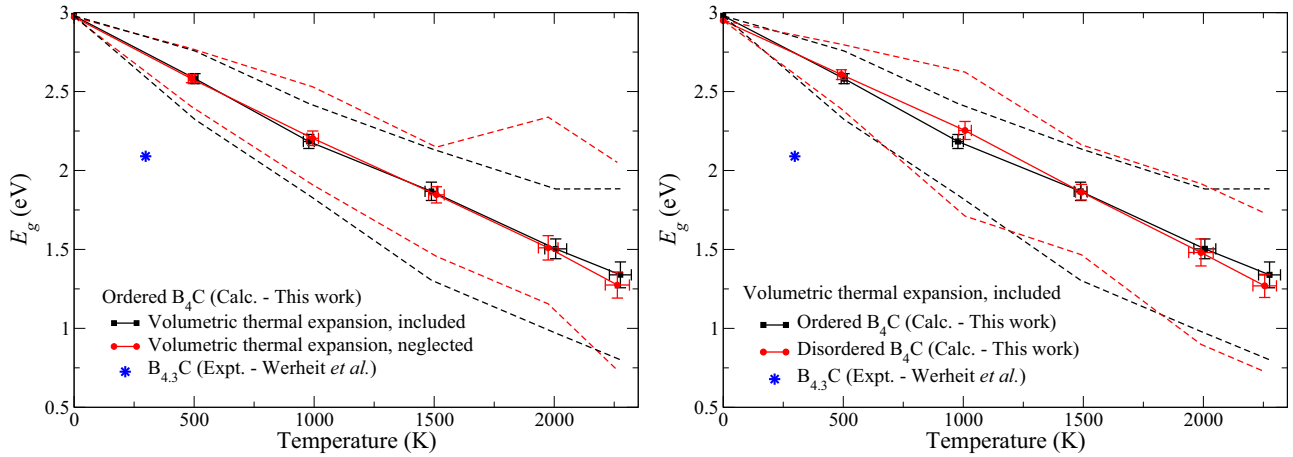

FIG. 4. GGA-PBE96 estimated mean values of electronic band gap, evaluated from the AIMD simulations equilibrated at 500, 1000, 1500, 2000, and 2250 K, of (a) ordered B_4C with and without inclusion of the volumetric thermal expansion, and (b) ordered and disordered B_4C taking into account the volumetric thermal expansions. The error bars represent the standard deviation at 95% confidence interval of the mean values of E_g and temperature, while the dashed lines indicate the maximum and minimum values of observed E_g among the 40 snapshots at the corresponding equilibration temperature. Blue stars in (a) and (b) denote the experimental band gap, derived from the optical measurements of $B_{4.3}C$ at ambient conditions [23].

behave like a semimetal, in which the band gap transforms into the electronic density of states minimum at the Fermi level [24]. The semimetallic properties have been attributed to the topologically disordered structure of amorphous B_4C, represented by a random icosahedral network connected with the amorphous B-C matrix cooperating with an absence of the intericosahedral linear CBC chains as well as clustering of carbon atoms [24].

B. Energetics and electronic band gap of $B_{4.3}C$

According to the description provided in Sec. II A, we introduce a small fraction of B_{12}(CBC) and $B_{12}(B_4)$ with the B_{12}(CBC)-to-$B_{12}(B_4)$ ratio of 2 into a matrix of $B_{11}C^p$(CBC) to make the composition of boron carbide $B_{4.3}C$, which is claimed to be the carbon-rich limit of the homogeneity range in experiment [36,37]. For this particular case, our model of $B_{4.3}C$ is composed of 90% $B_{11}C^p$(CBC), 6.67% B_{12}(CBC), and 3.33% $B_{12}(B_4)$, constructed within a supercell of $5 \times 3 \times 2$ primitive rhombohedral unit cells (451 atoms). As we have found in the previous section that both the volumetric thermal expansion and the configurational disorder of C^p atoms, residing in $B_{11}C^p$ icosahedra, do not have a significant impact on the band gap of B_4C, we neglect them in the following band-gap calculations of $B_{4.3}C$.

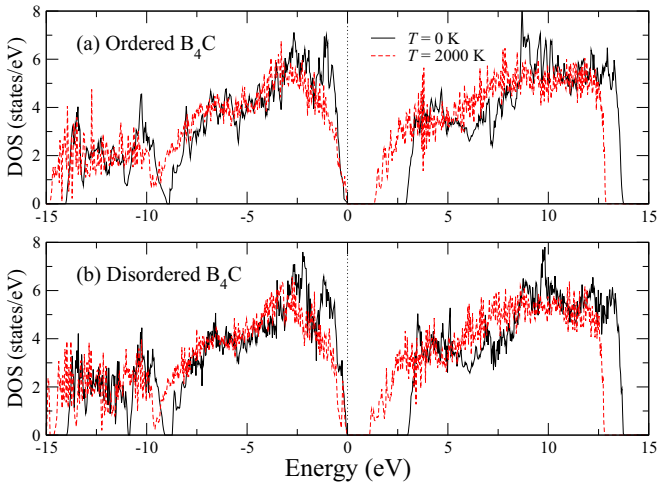

FIG. 5. Electronic density of states of (a) ordered B_4C and (b) disordered B_4C, taking into account the effect of volume expansion. Solid black lines are the density of states, calculated at 0 K, while dashed red lines represent the density of states, randomly chosen from 1 out of 40 snapshots of AIMD simulations equilibrated at 2000 K. Dotted lines at 0 eV indicate the highest occupied state.

Concerning the energetics of $B_{4.3}C$ with respect to that of B_4C, we find that the total energy at $T = 0$ K, derived from our structural model of $B_{4.3}C$ and subtracted by the chemical potential of the reference state given by α-rhombohedral boron, is comparable to that of ordered B_4C, and the energy difference between them is found to be less than 1 meV/atom. As a consequence, it is very likely that at elevated temperature $B_{4.3}C$ is thermodynamically stable over B_4C due to the entropy arising not only from the configurational disorder of C^p residing in $B_{11}C^p$ icosahedra, but also from the configurational disorder between $B_{11}C^p$(CBC), B_{12}(CBC), and $B_{12}(B_4)$. We note further that this could also be an explanation of why synthesizing boron carbide with the ideal stoichiometric composition of B_4C (20 at. % C), generally performed at high temperature, results in a mixture of boron carbide with a carbon content slightly lower than 20 at. %, i.e., $B_{\sim 4.3}C$, and free graphitelike carbon [61,62], and thus no successful synthesis of the ideally stoichiometric boron carbide B_4C has ever been reported.

Figure 6 shows the electronic density of states of $B_{4.3}C$, calculated at 0 and 500 K. We find that adding both B_{12}(CBC) and $B_{12}(B_4)$ with a ratio of 2:1 into a matrix of $B_{11}C^p$(CBC) to form $B_{4.3}C$ not only preserves the electrically semiconducting character of boron carbide but also gives rise to midgap states. As can be seen from Fig. 6, the unoccupied midgap states of

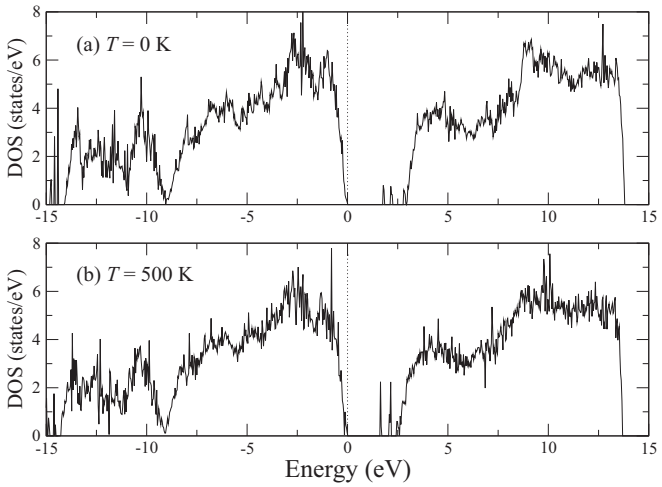

FIG. 6. Electronic density of states of $B_{4.3}C$, (a) calculated at 0 K and (b) randomly chosen from 1 out of 40 snapshots of AIMD simulations, equilibrated at 500 K. Dotted lines at 0 eV indicate the highest occupied state.

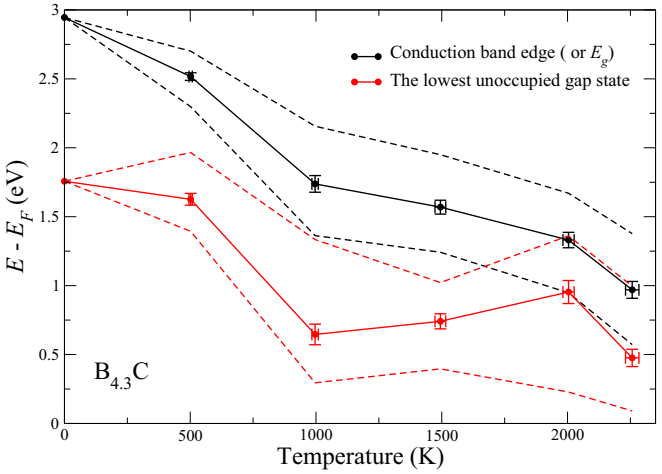

FIG. 7. GGA-PBE96 estimated mean positions of the conduction-band edge (solid black circles) and of the lowest unoccupied gap state (solid red circles), evaluated from the AIMD simulations of $B_{4.3}C$ equilibrated at 500, 1000, 1500, 2000, and 2250 K, with respect to the Fermi level (E_F) located at the valence-band edge. The error bars represent the standard deviation at 95% confidence interval of the mean values, while the dashed lines indicate the maximum and minimum values of the positions among the 40 snapshots during the AIMD simulations at the corresponding equilibration temperature.

$B_{4.3}C$ appear as the two sharply defined peaks in the band gap, and their origin is attributed to the presence of the rhombic B_4 chain. As demonstrated in the previous theoretical studies of boron carbide [31–35], one of the peaks is assigned as the split-off valence states, while the other peak appears as impurity states. As the concentration of $B_{12}(B_4)$ increases, the unoccupied defect states widen and form an impurity band, eventually overlapping with the conduction band. We note that the overlapping of the impurity band, arising from a high concentration of $B_{12}(B_4)$, with the conduction band was previously predicted for boron-rich boron carbide $B_{10.5}C$, represented by $[B_{12}(CBC)]_{0.67}[B_{12}(B_4)]_{0.33}$ [33–35]. However, in the dilute limit, the sharpness of these states indicates an impurity-band-type character.

At 0 K, the electronic band gap, defined by the distance between the valence-band edge and the conduction-band edge, of $B_{4.3}C$ is estimated to be 2.94 eV. This is similar to that of B_4C. The midgap states, however, appear at ∼1.7 eV above the valence-band edge, and this value would further reduce to ∼1.1 eV, if the effect of phonon-induced zero-point renormalization on the electronic band gap [57–59] was taken into account in the standard DFT-estimated band gap of $B_{4.3}C$. This would result in an underestimation of around 47% with respect to the experimental value, which is what would be expected from the standard DFT calculations, where the electronic exchange-correlation effects are derived within the generalized gradient approximation [20–22]. As a consequence, the appearance of the midgap states in $B_{4.3}C$, resulting from adding a small fraction of $B_{12}(CBC)$ and $B_{12}(B_4)$ into the matrix of $B_{11}C^p(CBC)$, provides a good description of the electronic band gap for carbon-rich boron carbide, which is also in line with the experiments [23,63,64].

Figure 7 illustrates the mean positions of the conduction-band edge and of the lowest unoccupied midgap state of $B_{4.3}C$, derived from the AIMD simulations, with respect to the position of the valence-band edge. We observe that, regardless of the gap states, the actual band gap of $B_{4.3}C$ decreases faster with increasing temperature as compared to that of B_4C. In addition, we find that the mean value of atomic displacements, induced by the lattice vibrations at a particular temperature, of $B_{4.3}C$ is larger than that of B_4C. For example, at 2000 K, the mean atomic displacement of $B_{4.3}C$ is 0.288 Å, while it is 0.208 Å for B_4C. These results could imply that the interatomic bonds in $B_{4.3}C$ are, on average, weaker than those of B_4C, and thus the temperature effects, such as thermal expansion, could be relatively stronger for $B_{4.3}C$.

IV. CONCLUSION

We have performed first-principles calculations to investigate the effect of temperature and configurational disorder on the electronic band gap of carbon-rich boron carbide, in particular B_4C represented by $B_{11}C^p(CBC)$. Our simulations reveal that the volumetric thermal expansion and the thermally induced configurational disorder of the icosahedral C^p atoms, residing in the $B_{11}C^p$ icosahedra, have a minimal impact on the electronic band gap of B_4C. At 298 K, the band gap of B_4C is estimated by standard density functional theory calculations to be 2.74 eV, overestimating the experimental band gap of 2.09 eV, obtained from the optical measurement of $B_{4.3}C$ [23], by approximately 31%. We, however, find that configurational disorder induced by introducing a small fraction of thermodynamically favorable $B_{12}(CBC)$ and $B_{12}(B_4)$ into the matrix of $B_{11}C^p(CBC)$ to achieve the composition of $B_{4.3}C$ leads to a smaller band gap of 1.7 eV due to the appearance of the midgap states. The existence of such structural motifs could thus resolve the previous discrepancies in terms of the electronic band gap of carbon-rich boron carbide between

experiment and theoretical calculations, carried out via standard DFT calculations of the idealized $B_{11}C^{p}$(CBC).

ACKNOWLEDGMENTS

The financial support by the Swedish Research Council (VR) through the international career Grant No. 2014-6336, Marie Sklodowska Curie Actions, Cofund, Project INCA 600398, and the Swedish Foundation for Strategic Research (SSF) through the Future Research Leaders 6 program is gratefully acknowledged by B.A. The financial support from Kungl. Ingenjörsvetenskapsakademiens Hans Werthén-Fond is gratefully acknowledged by A.E. S.I.S. acknowledges the Swedish Research Council (VR) Grant No. 2014-4750. B.A. and S.I.S. also acknowledge the support from the Swedish Government Strategic Research Area in Materials Science on Functional Materials at Linköping University (Faculty Grant SFO-Mat-LiU No. 2009 00971). The simulations were carried out using supercomputer resources provided by the Swedish National Infrastructure for Computing (SNIC) performed at the National Supercomputer Centre (NSC) and the Center for High Performance Computing (PDC).

[1] F. Thevénot, Boron carbide: A comprehensive review, J. Eur. Ceram. Soc. **6**, 205 (1990).
[2] V. Domnich, S. Reynaud, R. A. Haber, and M. Chhowalla, Boron carbide: Structure, properties, and stability under stress, J. Am. Ceram. Soc. **94**, 3605 (2011).
[3] H. Okamoto, B-C (boron-carbon), J. Phase Equilib. **13**, 436 (1992).
[4] H. K. Clark and J. L. Hoard, The crystal structure of boron carbide, J. Am. Chem. Soc. **65**, 2115 (1943).
[5] H. L. Yakel, The crystal structure of a boron-rich boron carbide, Acta Crystallogr. Sect. B **31**, 1797 (1975).
[6] B. Morosin, A. W. Mullendore, D. Emin, and G. A. Slack, in *Rhombohedral Crystal Structure of Compounds Containing Boron-Rich Icosahedra*, AIP Conf. Proc. No. 140 (AIP, New York, 1986), p. 70.
[7] B. Morosin, G. H. Kwei, A. C. Lawson, T. L. Aselage, and D. Emin, Neutron powder diffraction refinement of boron carbides. Nature of intericosahedral chains, J. Alloys Compd. **226**, 121 (1995).
[8] D. Emin, Unusual properties of icosahedral boron-rich solids, J. Solid State Chem. **179**, 2791 (2006).
[9] D. Emin, Icosahedral boron-rich solids, Phys. Today **40**, 55 (1987).
[10] T. L. Aselage, D. Emin, C. Wood, I. Mackinnon, and I. Howard, Anomalous Seebeck coefficient in boron carbides, MRS Proc. **97**, 27 (1987).
[11] H. Werheit, Boron-rich solids: A chance for high-efficiency high-temperature thermoelectric energy conversion, Mater. Sci. Eng., B **29**, 228 (1995).
[12] D. M. Bylander and L. Kleinman, Structure of $B_{13}C_2$, Phys. Rev. B **43**, 1487 (1991).
[13] M. Calandra, N. Vast, and F. Mauri, Superconductivity from doping boron icosahedra, Phys. Rev. B **69**, 224505 (2004).
[14] D. R. Armstrong, J. Bolland, P. G. Perkins, G. Will, and A. Kirfel, The nature of the chemical bonding in boron carbide. IV. Electronic band structure of boron carbide, $B_{13}C_2$, and the model of the structure $B_{12}C_3$, Acta Crystallogr. Sect. B **39**, 324 (1983).
[15] C. Wood and D. Emin, Conduction mechanism in boron carbide, Phys. Rev. B **29**, 4582 (1984).
[16] L. Zuppiroli, N. Papandreou, and R. Kormann, The dielectric response of boron carbide due to hopping conduction, J. Appl. Phys. **70**, 246 (1991).
[17] D. M. Bylander, L. Kleinman, and S. Lee, Self-consistent calculations of the energy bands and bonding properties of $B_{12}C_3$, Phys. Rev. B **42**, 1394 (1990).
[18] K. Shirai, Electronic structures and mechanical properties of boron and boron-rich crystals (Part I), J. Superhard Mater. **32**, 205 (2010).
[19] A. Ektarawong, S. I. Simak, L. Hultman, J. Birch, and B. Alling, First-principles study of configurational disorder in B_4C using a superatom-special quasirandom structure method, Phys. Rev. B **90**, 024204 (2014).
[20] J. P. Perdew and M. Levy, Physical Content of the Exact Kohn-Sham Orbital Energies: Band Gaps and Derivative Discontinuities, Phys. Rev. Lett. **51**, 1884 (1983).
[21] G. Onida, L. Reining, and A. Rubio, Electronic excitations: Density-functional versus many-body Green's-function approaches, Rev. Mod. Phys. **74**, 601 (2002).
[22] P. J. Hasnip, K. Refson, M. I. J. Probert, J. R. Yates, S. J. Clark, and C. J. Pickard, Density functional theory in the solid state, Philos. Trans. R. Soc. A **372**, 20130270 (2014).
[23] H. Werheit, On excitons and other gap states in boron carbide, J. Phys.: Condens. Matter **18**, 10655 (2006).
[24] V. I. Ivashchenko and V. I. Shevchenko, First-principles study of the atomic and electronic structures of crystalline and amorphous B_4C, Phys. Rev. B **80**, 235208 (2009).
[25] J. Heyd, G. E. Scuseria, and M. Ernzerhof, Hybrid functionals based on a screened Coulomb potential, J. Chem. Phys. **118**, 8207 (2003).
[26] J. Heyd and G. E. Scuseria, Efficient hybrid density functional calculations in solids: Assessment of the Heyd-Scuseria-Ernzerhof screened Coulomb hybrid functional, J. Chem. Phys. **121**, 1187 (2004).
[27] J. Heyd, G. E. Scuseria, and M. Ernzerhof, Erratum: Hybrid functionals based on a screened Coulomb potential [J. Chem. Phys. **118**, 8207 (2003)] **124**, 219906 (2006).
[28] H. Werheit, Are there bipolarons in icosahedral boron-rich solids?, J. Phys.: Condens. Matter **19**, 186207 (2007).
[29] M. M. Balakrishnarajan, P. D. Pancharatna, and R. Hoffmann, Structure and bonding in boron carbide: The invincibility of imperfections, New J. Chem. **31**, 473 (2007).
[30] A. Ektarawong, S. I. Simak, L. Hultman, J. Birch, and B. Alling, Configurational order-disorder induced metal-nonmetal transition in $B_{13}C_2$ studied with first-principles superatom-special quasirandom structure method, Phys. Rev. B **92**, 014202 (2015).
[31] K. Shirai, K. Sakuma, and N. Uemura, Theoretical study of the structure of boron carbide $B_{13}C_2$, Phys. Rev. B **90**, 064109 (2014).
[32] K. Rasim, R. Ramlau, A. Leithe-Jasper, T. Mori, U. Burkhardt, H. Borrmann, W. Schnelle, C. Carbogno, M. Scheffler, and Y.

Grin, Local atomic arrangements and band structure of boron carbide, Angew. Chem. **130**, 1 (2018).

[33] K. Rasim, C. Carbogno, R. Ramlau, A. Leithe-Jasper, T. Mori, H. Borrmann, U. Burkhard, W. Schnelle, M. Scheffler, and Y. Grin, A comprehensive study of intrinsic defects in boron carbide, Proceedings of the 19th International Symposium on Boron, Borides and Related Materials (ISBB), Freiburg, Germany, 2017 (unpublished).

[34] K. Rasim, C. Carbogno, and Y. Grin, Intrinsic defects in boron carbide: A comprehensive first-principles study (unpublished).

[35] A. Ektarawong, S. I. Simak, and B. Alling, Structural models of increasing complexity for icosahedral boron carbide with compositions throughout the single-phase region from first principles, Phys. Rev. B **97**, 174104 (2018).

[36] K. A. Schwetz and P. Karduck, *Investigations in the Boron-Carbon System with the Aid of Electron Probe Microanalysis*, AIP Conf. Proc. No. 231 (AIP, New York, 1991), p. 405.

[37] H. Werheit and S. Shalamberidze, Advanced microstructural of boron carbide, J. Phys.: Condens. Matter **24**, 385406 (2012).

[38] I. Jiménez, D. G. Sutherland, T. van Buuren, J. A. Carlisle, L. J. Terminello, and F. J. Himpsel, Photoemission and x-ray absorption study of boron carbide and its surface thermal stability, Phys. Rev. B **57**, 13167 (1998).

[39] V. F. Sears, Neutron scattering lengths and cross sections, Neutron News **3**, 26 (1992).

[40] J. E. Saal, S. Shang, and Z. K. Liu, The structural evolution of boron carbide via ab initio calculations, Appl. Phys. Lett. **91**, 231915 (2007).

[41] N. Vast, J. Sjakste, and E. Betranhandy, Boron carbides from first principles, J. Phys.: Conf. Ser. **176**, 012002 (2009).

[42] M. Widom and W. P. Huhn, Prediction of orientational phase transition in boron carbide, Solid State Sci. **14**, 1648 (2012).

[43] S. Yao, W. P. Huhn, and M. Widom, Phase transitions of boron carbide: Pair interaction model of high carbon limit, Solid State Sci. **47**, 21 (2015).

[44] S. Yao, Q. Gao, and M. Widom, Phase diagram of boron carbide with variable carbon composition, Phys. Rev. B **95**, 054101 (2017).

[45] A. Ektarawong, S. I. Simak, and B. Alling, Carbon-rich icosahedral boron carbides beyond B_4C and their thermodynamic stabilities at high temperature and pressure from first principles, Phys. Rev. B **94**, 054104 (2016).

[46] P. E. Blöchl, Projector augmented-wave method, Phys. Rev. B **50**, 17953 (1994).

[47] G. Kresse and J. Furthmüller, Efficiency of ab-initio total energy calculations for metals and semiconductors using a plane-wave basis set, Comput. Mater. Sci. **6**, 15 (1996).

[48] G. Kresse and J. Furthmüller, Efficient iterative schemes for *ab initio* total-energy calculations using a plane-wave basis set, Phys. Rev. B **54**, 11169 (1996).

[49] J. Perdew, K. Burke, and M. Ernzerhof, Generalized Gradient Approximation Made Simple, Phys. Rev. Lett. **77**, 3865 (1996).

[50] H. J. Monkhorst and J. D. Pack, Special points for Brillouin-zone integrations, Phys. Rev. B **13**, 5188 (1976).

[51] A. Togo and I. Tanaka, First principles phonon calculations in materials science, Scr. Mater. **108**, 1 (2015).

[52] A. Togo, F. Oba, and I. Tanaka, First-principles calculations of the ferroelastic transition between rutile-type and $CaCl_2$-type SiO_2 at high pressures, Phys. Rev. B **78**, 134106 (2008).

[53] S. Nosé, Constant temperature molecular dynamics methods, Prog. Theor. Phys. Suppl. **103**, 1 (1991).

[54] P. E. Blöchl, O. Jepsen, and O. K. Andersen, Improved tetrahedron method for Brillouin-zone integrations, Phys. Rev. B **49**, 16223 (1994).

[55] H. L. Yakel, Lattice expansions of two boron carbides between 12 and 940 °C, J. Appl. Crystallogr. **6**, 471 (1973).

[56] G. V. Tsagareishvili, T. G. Nakashidze, J. Sh. Jobava, G. P. Lomidze, D. E. Khulelidze, D. Sh. Tsagareishvili, and O. A. Tsagareishvili, Thermal expansion of boron and boron carbide, J. Less-Common Met. **117**, 159 (1986).

[57] F. Giustino, S. G. Louie, and M. L. Cohen, Electron-Phonon Renormalization of the Direct Band Gap of Diamond, Phys. Rev. Lett. **105**, 265501 (2010).

[58] G. Antonius, S. Poncé, P. Boulanger, M. Côté, and X. Gonze, Many-Body Effects on the Zero-Point Renormalization of the Band Structure, Phys. Rev. Lett. **112**, 215501 (2014).

[59] R. Tutchton, C. Marchbanks, and Z. Wu, Structural impact on the eigenenergy renormalization for carbon and silicon allotropes and boron nitride polymorphs, Phys. Rev. B **97**, 205104 (2018).

[60] H. Dekura, K. Shirai, and A. Yanase, Metallicity of boron carbides at high pressure, J. Phys. Conf. Ser. **215**, 012117 (2010).

[61] C. Pallier, J.-M. Leyssale, L. A. Truflandier, A. T. Bui, P. Weisbecker, C. Gervais, H. E. Fischer, F. Sirotti, F. Teyssandier, and G. Chollon, Structure of an amorphous boron carbide film: An experimental and computational approach, Chem. Mater. **25**, 2618 (2013).

[62] J. K. Sonber, T. S. R. Ch. Murthy, C. Subramanian, R. K. Fotedar, R. C. Hubli, and A. K. Suri, Synthesis, densification and characterization of boron carbide, Trans. Ind. Ceram. Soc. **72**, 100 (2013).

[63] H. Werheit, H. W. Rotter, S. Shalamberidze, A. Leithe-Jasper, and T. Tanaka, Gap-state related photoluminescence in boron carbide, Phys. Status Solidi B **248**, 1275 (2011).

[64] H. Werheit, V. Filipov, U. Schwarz, M. Armbrüster, A. Leithe-Jasper, T. Tanaka, and S. O. Shalamberidze, On surface Raman scattering and luminescence radiation in boron carbide, J. Phys.: Condens. Matter **22**, 045401 (2010).